



Effect of ultrasonic compound cutting on the microstructure and properties of formed chip

Haimeng Sun¹ · Feng Jiao¹ · Ying Niu¹ · Zhuangfei Wang¹

Received: 17 August 2021 / Accepted: 28 March 2022 / Published online: 2 April 2022
© The Author(s), under exclusive licence to Springer-Verlag London Ltd., part of Springer Nature 2022

Abstract

Severe plastic deformation (SPD) with high strain rate can increase the material dislocation density, reduce the grain size, and improve the mechanical properties. In this article, ultrasonic compound cutting (UCC) was proposed to improve the efficiency of preparing ultra-fine grain (UFG) pure copper by SPD methods. The motion characteristics and strain rate model of UCC were analyzed, and it was concluded that the maximum strain rate in the primary shear zone can be increased by ultrasonic vibration. According to the 3D FEM equivalent model of UCC, the UCC and traditional compound cutting (TCC) were compared and analyzed from the perspective of strain rate. The simulation results showed that the strain rate in the shear zone of UCC was significantly larger than that of TCC. The microstructure and mechanical properties of pure copper chip were studied by using a self-developed machining device. The experiment results showed that the grain refinement, dislocation density, and microhardness of pure copper chip were significantly improved in UCC. When the ultrasonic amplitude was 3 μm , the UCC chip grains were about 2.66 μm and the hardness reached 124 HV, which was about 8% higher than the TCC chip. The findings of this research provide an important reference for machining UFG pure copper with enhanced mechanical properties.

Keywords Pure copper · Ultrasonic compound cutting · 3D FEM equivalent model · Microstructure · Mechanical properties

1 Introduction

Microelectro-mechanical system (MEMS) plays an important role in modern industry and is widely used in biomedicine, electronic communication and aerospace fields. The rapid rise of MEMS has driven the current industry towards miniaturization and micromation [1]. In MEMS, if traditional materials are used to produce microparts, the average grain size is usually above 10 μm , which is the same as the characteristic size of most microparts. This will cause size effect and reduce the dimensional accuracy and service life of parts [2]. Ultra-fine grain (UFG) materials have attracted widespread attention for their excellent properties such as high strength, high toughness, lower ductile–brittle transition temperature, high strain rate, and low temperature superplasticity, etc. [3]. If UFG materials are applied

to microparts, the overall performance of MEMS will be improved. Pure copper is widely used in MEMS as an important basic material and functional material. At the same time, UFG pure copper has high strength, ductility, electrical and thermal conductivity, and fatigue properties [4, 5]. Therefore, the preparation of UFG pure copper and the study of its microstructure and properties have become current research hotspots.

Severe plastic deformation (SPD) can effectively refine the internal structure of materials by applying large shear strain to produce UFG materials with large angular grain boundaries, and the grain size can be refined to several hundred nanometers. SPD methods including equal channel angular pressing (ECAP) [6], high-pressure torsion (HPT) [7], accumulative roll bonding (ARB) [8], and cyclic extrusion compression (CEC) [9] are therefore employed to produce UFG materials. SPD can significantly increase the density of metals and alloys, eliminate internal defects in materials, and make it difficult to cause pores and pollution in machining. However, SPD has many limitations. Firstly, due to the limitations of forming equipment, the strain rate

✉ Ying Niu
niuying@hpu.edu.cn

¹ Henan Polytechnic University, Jiaozuo, China

of SPD machining is very small ($< 10^2 \text{ s}^{-1}$) and the temperature in deformation zone is also very low, so SPD is difficult to deform medium and high-strength alloys. Secondly, SPD needs multiple machining to produce large strain, which will lead to uncertainty in the control of deformation parameters (e.g., strain, strain rate) and deformation paths [10].

Among these SPD techniques, large strain extrusion machining (LSEM) [11] is an attractive method for preparing UFG materials. It not only imposes large shear strain on materials in a single pass, but also has unique advantages in controlling chip forming and continuous production. Saldana et al. [12] used LSEM and micro-EDM technology to prepare LSEM chips into nickel-based superalloy Inconel 718 small-scale gears. The measurement results showed that the shape accuracy and tolerance of the gear were very high, and the nanoscale microstructure and enhanced mechanical properties were retained in the gear. LSEM can directly prepare chip waste into UFG formed strips with industrial demand, which can be further processed into MEMS microparts.

At present, the demand for high-performance industrial materials is growing rapidly, so scholars have begun to introduce ultrasonic vibration assisted technology to prepare UFG materials. Ultrasonic vibration machining can improve the traditional manufacturing processes, and make significant changes in mechanical properties, micromorphology, surface integrity, and fatigue properties of materials [13, 14]. Ahmadi et al. [15] designed an ultrasonic-assisted ECAP system, and the punch could be excited by ultrasonic vibration. The results showed that the grains of pure aluminum samples were refined to $45 \mu\text{m}$ in ECAP machining. When the amplitude was $2.5 \mu\text{m}$ and $5 \mu\text{m}$, the material grains were refined to $28.2 \mu\text{m}$ and $22 \mu\text{m}$, respectively. It was proved that ultrasonic vibration can significantly improve the grain refinement of pure aluminum. Zhang et al. [16] used shot peening and ultrasonic shot peening to machine 7075-T651 aluminum alloy. The results showed that the surface roughness in ultrasonic shot peening was reduced by 35.5%, and the surface hardness was increased by about 31.9%. Cheng et al. [17] carried out an ultrasonic rolling experiment with 45 steel. When the amplitude increased from 0 to $6 \mu\text{m}$, the depth of structure refinement increased from 17 to $53.5 \mu\text{m}$. The results indicated that ultrasonic vibration rolling can effectively refine the internal structure of 45 steel. A large number of literatures show that under the same conditions, if ultrasonic vibration is added to SPD, the grain refinement on the material surface will increase and a thicker nanostructure layer will be formed. At the same time, the mechanical properties of materials are significantly improved, and the combination of ultrasonic vibration and SPD can obtain better results than traditional machining methods [18, 19]. We found that there was no research on the combination of

LSEM and ultrasonic vibration by reading literature, so we proposed the UCC method in this article.

In this article, a new ultrasonic compound cutting (UCC) method was proposed on the basis of LSEM. According to the motion characteristics and strain rate model of UCC, the effect of ultrasonic vibration on the strain rate in the primary shear zone was analyzed. The 3D FEM equivalent model of UCC was established, and the differences between traditional compound cutting (TCC) and UCC were compared and analyzed from the viewpoint of strain rate. The microstructure features and mechanical properties were characterized by employing optical microscopy (OM), scanning electron microscope (SEM), Vickers microhardness tester, and X-ray diffraction (XRD). The main concerns of this paper include (i) developing a new strategy to prepare UFG pure copper with enhanced mechanical properties, (ii) exploring the relationships between hardness and microstructure of the UCC samples, and (iii) revealing the effect of strain rate on the machining results.

2 Theoretical model of UCC strain rate

2.1 Motion characteristics analysis of UCC

In the machining process, a unit on the cutting edge is taken to establish the cutting edge path equation. In TCC, the cutting edge path equation is as follows:

$$\begin{cases} X'(t) = (r - a_p) \cdot \sin(2\pi nt/60) \\ Y'(t) = (r - a_p) \cdot \cos(2\pi nt/60) \\ Z'(t) = v_f \cdot t \end{cases} \quad (1)$$

where r is the radius of workpiece, a_p is the cutting depth, n is the spindle speed, and v_f is the feed speed of cutting tool.

In the UCC process, the cutting edge path equation in one vibration period is as follows:

$$\{ Y(t) = A_Y \sin(2\pi ft) \quad (2)$$

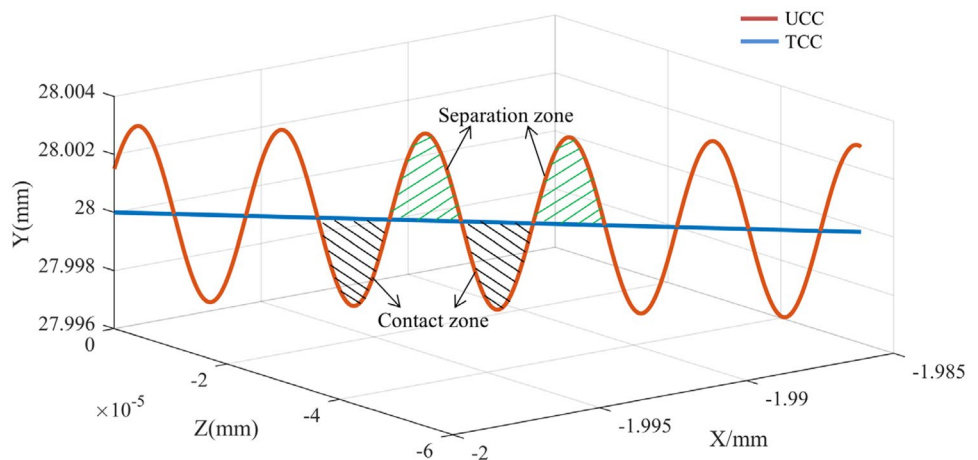
where A_Y is the amplitude of ultrasonic longitudinal vibration and f is the ultrasonic vibration frequency.

UCC is based on the TCC, which applies periodic vibration with the same frequency in the cutting direction. The cutting edge path equation of UCC is as follows:

$$\begin{cases} X'(t) = (r - a_p) \cdot \sin(2\pi nt/60) \\ Y'(t) = (r - a_p) \cdot \cos(2\pi nt/60) + A_Y \sin(2\pi ft) \\ Z'(t) = v_f \cdot t \end{cases} \quad (3)$$

The comparison of cutting edge trajectory between TCC and UCC is shown in Fig. 1. Due to the effect of ultrasonic

Fig. 1 Comparison of cutting edge trajectory between TCC and UCC



high-frequency vibration, the cutting edge and the workpiece are periodically separated and contacted. This special movement will make the chip get different plastic deformation from TCC in the machining process.

2.2 Strain rate model of UCC

TCC is an alteration of conventional orthogonal machining, which can be considered as a shear plane strain process. The chip thickness in orthogonal machining is formed freely, while it is set as a prior in TCC. The main form of deformation in machining is the shear slip of materials. The chip is mainly affected by two deformation zones in TCC machining, including the primary shear zone (the first deformation zone), the extrusion, and friction zone of tool and material (the second deformation zone). The schematic diagram of TCC shear deformation and the associated geometric parameters are shown in Fig. 2.

The shear strain imposed on the chip during the chip formation in TCC is calculated by:

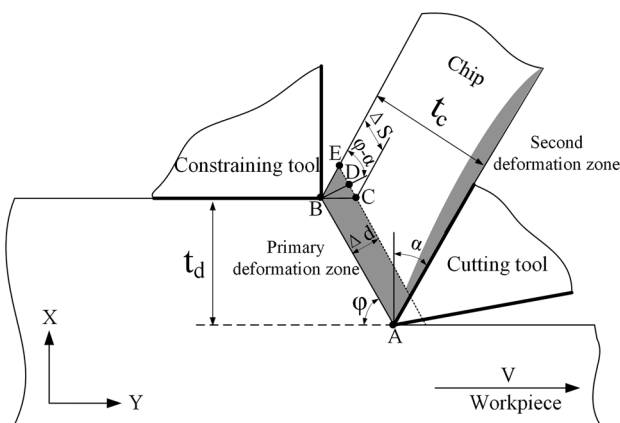


Fig. 2 Schematic diagram of TCC shear deformation and associated geometric parameters

$$\gamma = \frac{\Delta S}{\Delta d} = \frac{CE}{BD} = \frac{CD + DE}{BD} = \cot\varphi + \tan(\varphi - \alpha) \quad (4)$$

where φ is the shear angle and α is the tool rake angle.

In order to characterize the deformation degree of chip, the chip compression ratio λ is introduced:

$$\lambda = \frac{t_c}{t_d} = \frac{AB\sin(90^\circ - \varphi + \alpha)}{AB\sin\varphi} \quad (5)$$

From Eq. (5):

$$\tan\varphi = \frac{\cos\alpha}{\lambda - \sin\alpha} \quad (6)$$

From Eqs. (4) to (6), the relationship between γ and λ can be obtained as follows:

$$\gamma = \frac{\lambda^2 - 2\lambda\sin\alpha + 1}{\lambda\cos\alpha} = \frac{\lambda}{\cos\alpha} + \frac{1}{\lambda\cos\alpha} - 2\tan\alpha \quad (7)$$

In general, the approximation of the deformation zone as a “shear plane,” albeit of small thickness (Δd), is a reasonable model and is applied in the present study to estimate the strain rate. Then, the strain rate [20, 21] under localized deformation can be approximated as:

$$\dot{\epsilon} = \frac{\gamma}{\Delta t} = \frac{\Delta s}{\Delta d \Delta t} = \frac{V_s}{\Delta d} \quad (8)$$

where V_s is the shear speed and Δd is the primary deformation zone (PDZ) thickness, which is typically taken as 50 μm using the particle image velocimetry (PIV) technique [22, 23].

The shear plane model is shown in Fig. 3. ABCD is the primary deformation zone, V is the cutting speed, V_c is the chip speed, and V_s is the shear speed. V , V_c , and V_s can form a closed vector graph. The shear speed [24] is calculated by:

$$V_s = \frac{\cos\alpha}{\cos(\varphi - \alpha)} V \quad (9)$$

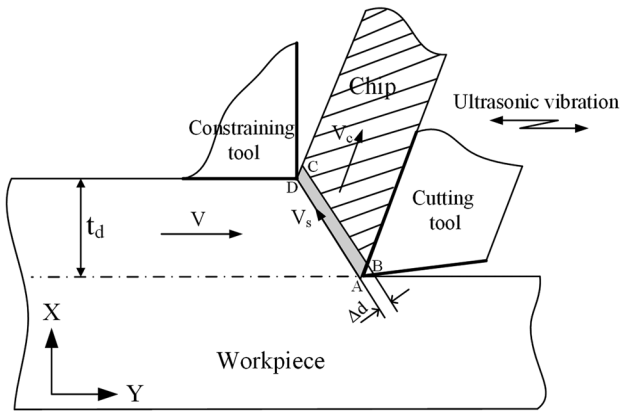


Fig. 3 The shear plane model

The cutting speed V can be obtained from Eq. (3):

$$V(t) = \frac{\pi n(r - a_p)}{30} \cdot \cos(2\pi n t / 60) + 2\pi f A_y \cdot \sin(2\pi f t) \quad (10)$$

From Eqs. (8), (9) and (10), the maximum strain rate of UCC can be obtained as follows:

$$\dot{\epsilon}_{\max} = \frac{\cos\alpha}{\cos(\varphi - \alpha)\Delta d} \cdot \left[\frac{\pi n(r - a_p)}{30} \cdot \cos(2\pi n t / 60) + 2\pi f A_y \cdot \sin(2\pi f t) \right] \quad (11)$$

From Eq. (11), it can be obtained that the maximum strain rate $\dot{\epsilon}_{\max}$ in UCC is proportional to the ultrasonic amplitude A_y . The grain refinement is not only related to the strain of plastic deformation of materials, but also to the strain rate, so the result of UCC at high strain rate will be more excellent.

Fig. 4 Finite element model of UCC

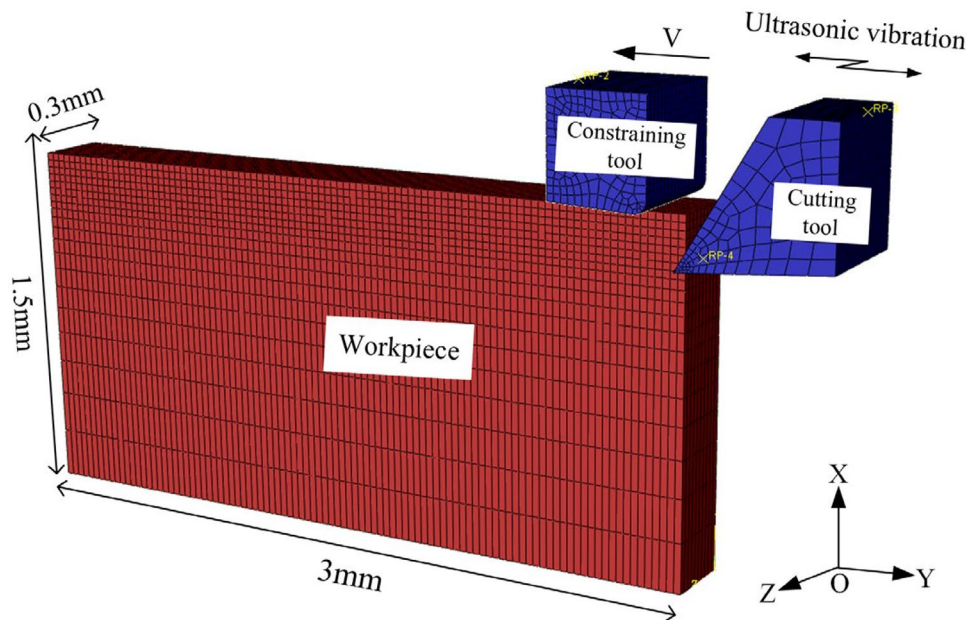


Table 1 Material properties of pure copper [3]

Parameters	Reference value
Density/(kg/m ³)	8960
Yang's model/GPa	108
Poisson's ratio	0.333
Specific heat capacity/(J/kg · K)	3.16032
Melting point/K	1356
Thermal conductivity/(W/(m · K))	122.613
Expansion coefficient/(μm/(m·K))	17.5

3 Simulation and validation of UCC strain rate

3.1 FEM details

FEM is adopted to simulate machining with great success. The 3D model of the cutting tool, constraining tool, and workpiece are shown in Fig. 4. The tool material is carbide, and the workpiece material is pure copper; the material properties of workpiece are shown in Table 1 [3]. In order to realize the ultrasonic vibration of the cutting tool and constraining tool, the reference points of the combined tool are given a cutting speed and periodic displacement along the cutting direction.

The key to ensure the accuracy of UCC simulation is the constitutive model. The Johnson–cook constitutive model is able to express strain hardening, strain rate strengthening, and thermal softening at high strain rate, which is more consistent with actual machining. So J-C constitutive model and J-C failure criteria are adopted in this article. The J-C constitutive

Table 2 J-C constitutive model parameters of pure copper [25]

A	B	C	m	n	$\dot{\epsilon}_0$	T_r	T_m
90	292	0.025	1.09	0.31	1	300	1356

model parameters and failure criteria parameters of pure copper are shown in Tables 2 and 3, respectively [25].

3.2 Simulation results and analysis of strain rate

In order to investigate how the ultrasonic vibration affects material properties and microstructure, the correlation between the machining parameters (e.g., amplitude) and deformation parameters (e.g., strain rate) is required. The literature shows that at high strain rate, the dislocation distribution will be more random and uniform and the grain size will also decrease [26, 27]. Therefore, the study of chip deformation zone strain rate is of guiding significance for the production of UFG pure copper.

The strain rate distribution in the chip with different ultrasonic amplitudes is shown in Fig. 5. The strain rate is changed by the variation in amplitude: strain rate is low at small amplitude and increases with the increase of amplitude. The maximum values of strain rate are 1.636×10^4 , 3.72×10^4 , 3.996×10^4 , and 5.482×10^4 , corresponding to the four amplitudes from 0 to 3 μm . When A_Y is 3 μm , the strain rate is maximum. The maximum value of strain rate increases from 1.636×10^4 to 3.72×10^4 as A_Y increases from 0 to 1 μm , representing a difference value of 2.084×10^4 . It shows that ultrasonic vibration can more significantly

Table 3 J-C failure criteria parameters of pure copper [25]

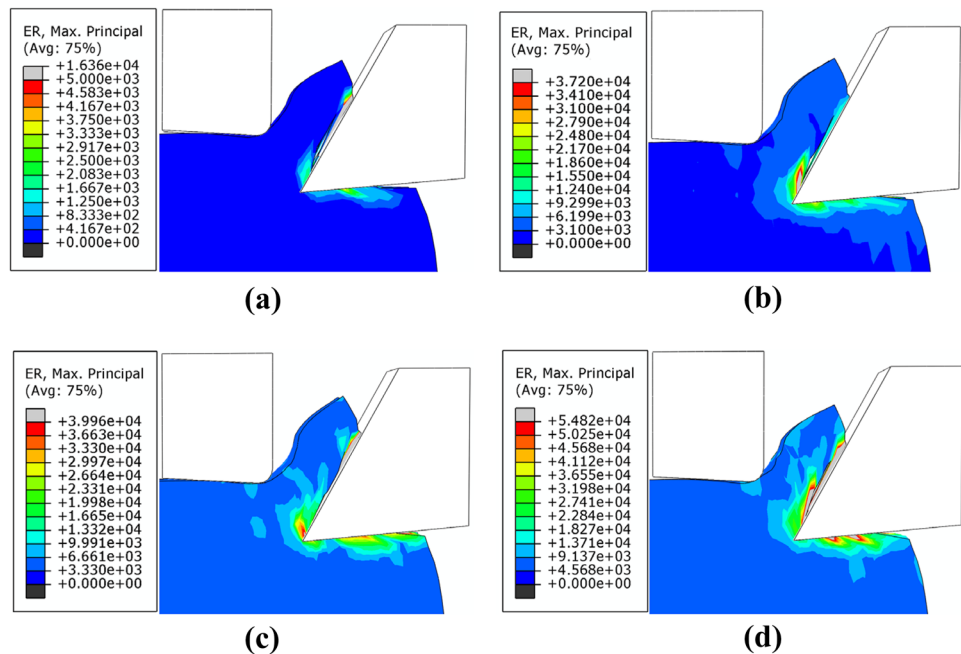
D_1	D_2	D_3	D_4	D_5
1.08	4.89	3.03	0.014	1.12

increase the strain rate in the deformation zone. The maximum value of strain rate increases from 3.72×10^4 to 3.996×10^4 as A_Y increases from 1 to 2 μm , representing a difference value of 0.276×10^4 . However, it increases from 3.996×10^4 to 5.482×10^4 , while A_Y increases from 2 to 3 μm , with a difference of 1.486×10^4 . The results show that the strain rate increases with the increase of the amplitude.

The strain rate changes with different ultrasonic amplitudes are shown in Fig. 6. The same point on workpiece is selected to compare the strain rate change. The simulation results show that as the cutting time increases, the strain rate curve gradually increases and the maximum strain rate will gradually increase with the increase of amplitude A_Y .

The effect of strain rate on refining the internal structure and modifying the surface structure cannot be ignored. When the material is mechanically deformed to produce high-density dislocation, the internal structure will be refined and the surface structure will be modified. The increase of dislocation density is not only related to the strain of plastic deformation, but also to the strain rate. The simulation results show that the maximum strain rate of ultrasonic compound cutting ($A_Y = 3 \mu\text{m}$) increases by about 2.3 times compared with traditional compound cutting, so the ultrasonic vibration technology can significantly increase the cutting strain rate.

Fig. 5 The distribution of strain rate with different ultrasonic amplitudes: **a** $A_Y = 0 \mu\text{m}$, **b** $A_Y = 1 \mu\text{m}$, **c** $A_Y = 2 \mu\text{m}$, and **d** $A_Y = 3 \mu\text{m}$



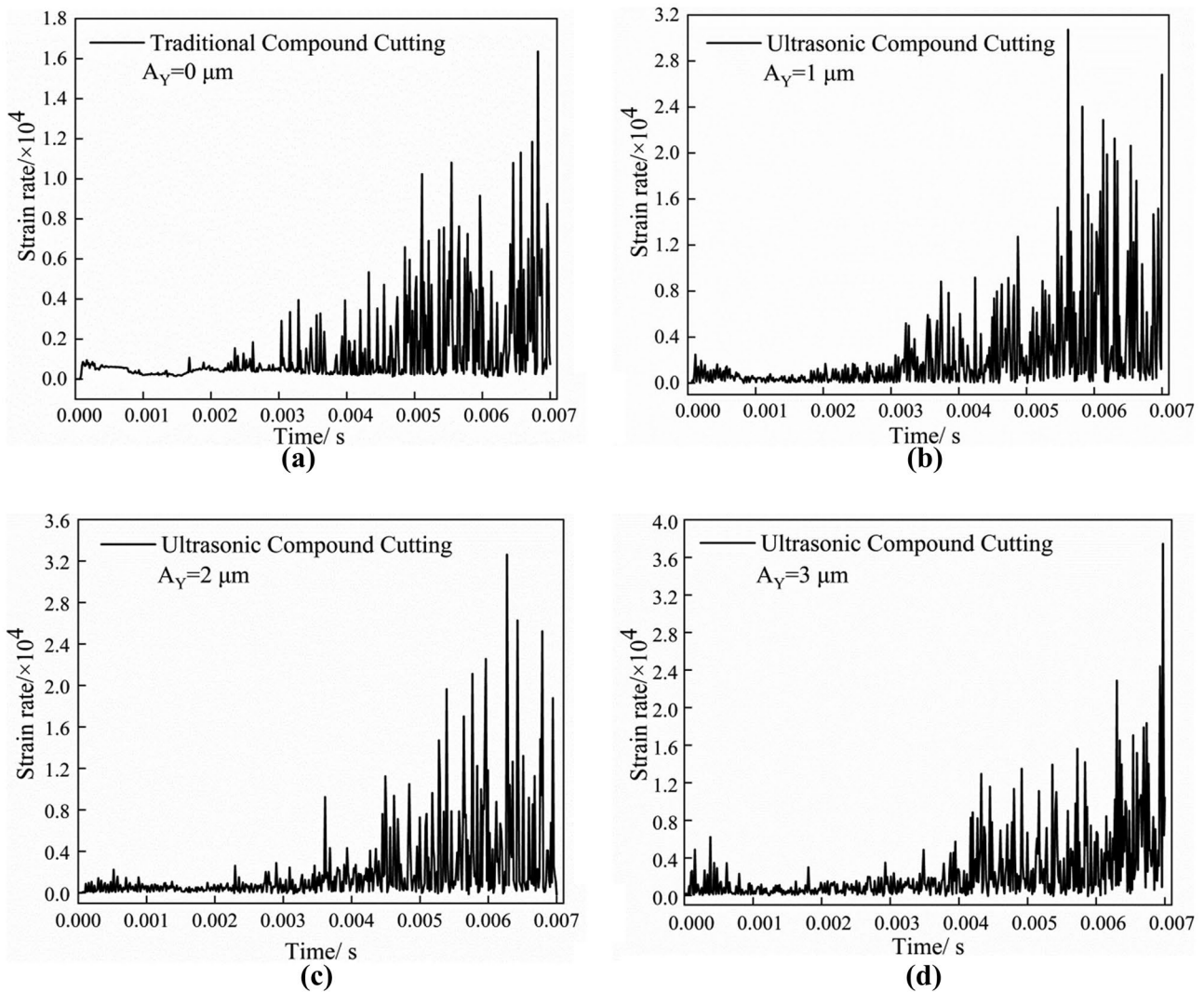


Fig. 6 Strain rate changes with different ultrasonic amplitudes: **a** $A_Y = 0\mu\text{m}$, **b** $A_Y = 1\mu\text{m}$, **c** $A_Y = 2\mu\text{m}$, and **d** $A_Y = 3\mu\text{m}$

4 Microstructure and properties experiment of UCC

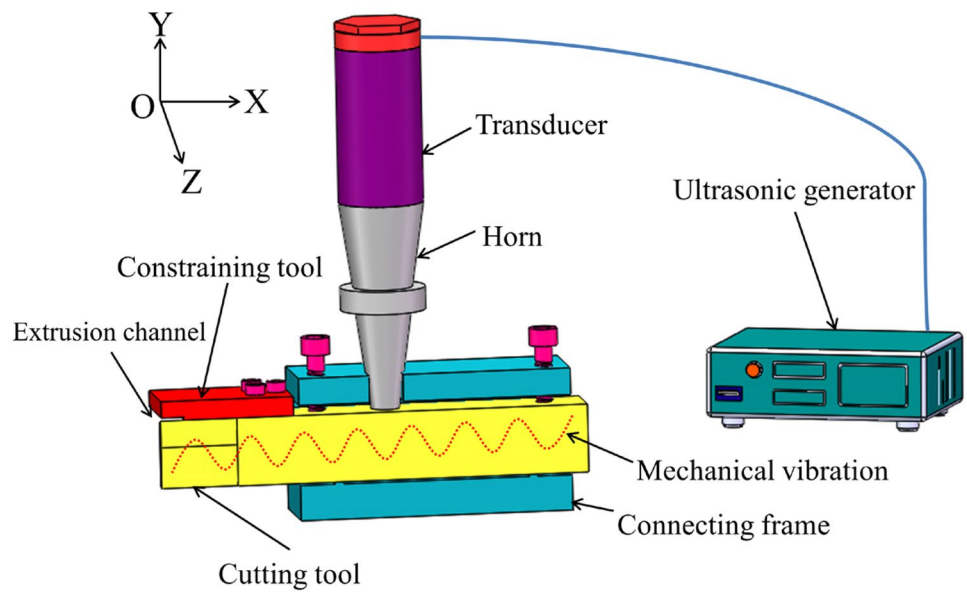
4.1 Experimental details

The experiment setup is shown in Fig. 7. The experiment setup is composed of high-frequency vibration system and extrusion cutting system. The high-frequency vibration system is composed of ultrasonic generator, transducer, and horn; the extrusion cutting system is composed of cutting tool, constraining tool, and connecting frame. The two systems cooperate with each other to generate ultrasonic high-frequency vibration for the cutting tool and constraining tool. The output amplitude of the system can be changed by adjusting the frequency and output power of the ultrasonic generator. At the same time, the frequency and current value of the numerical control panel of the ultrasonic generator are in a very small range to keep the amplitude constant.

The test conditions in this article are shown in Table 4. In order to minimize the influences of strain rate and temperature variations, the cutting speed is kept slow, and the work material is continuously fed into the extrusion channel with formation of the geometrically controlled chip. In order to ensure 2D deformation, the chip width is kept much larger than the thickness of the unformed chip. At that time, the strain along the chip width direction is minimal. All machining experiments are conducted on a universal lath (CA6140B/A), using machining oil (SAE-30) as lubricant and coolant. The commercial pure copper circular tube with the length of 200 mm, the outer diameter of 60 mm, and the thickness of 10 mm is served as the experimental material. The experimental setup of UCC is illustrated in Fig. 8.

As illustrated in Fig. 9, a laser displacement sensor, KEYENCE LK-G10, is used to measure the ultrasonic longitudinal amplitude of the combined tool. The laser beam of the laser displacement sensor is focused on the tool tip, and the value of

Fig. 7 Schematic diagram of UCC setup



the ultrasonic amplitude is read by PC. Microstructures of all samples are examined in detail using the OM and SEM. For this purpose, the samples are mechanically polished with abrasive paper of 600, 1000, 1500, 2000, and 3000 grit in sequence, followed by fine polishing with the diamond paste of 1 μm to the mirror finish. Grinding of the chip is started from the surface coming in contact with the tool rake face. Reagent (5 g $FeCl_3$, 50 mL HCl, and 100 mL H_2O) is adopted to etch the samples. As for SEM study, in order to avoid the decrease of conductivity affecting the observation result, so the samples are sprayed with gold. The formation of different phases of the samples is analyzed using XRD by scanning in the range 2θ 20–90°. θ - 2θ accurate scans with a step size of 0.02° are performed at room temperature. Microhardness tests are carried out with a Vickers microhardness tester at a load of 50 g for a dwell time of 15 s. An average value is taken from at least 15 readings for each sample. The test positions of OM, SEM, XRD, and microhardness are chosen on the plane closed to the tool rake face.

4.2 Experimental results and analysis of microstructure

OM images of the starting material and samples subjected to UCC are illustrated in Fig. 10. The OM image of the starting

material is shown in Fig. 10a, and the OM image processed by the image-pro-plus (IPP) software is shown in Fig. 10b. The microstructure of starting material mainly consists of grains in the range of 10–30 μm with a mean grain size of 18.15 μm, and grains larger than 50 μm can also be observed.

The OM images of UCC samples are shown in Fig. 10c–f. After UCC process, the grains of pure copper chip are highly refined. The IPP software is not easy to capture grain boundaries, so the linear intercept method [28] is used, and the equation is as follows:

$$\bar{l} = \frac{L}{P_i} \tag{12}$$

where \bar{l} is the average intersection length, L is the length of test line, and P_i is the number of intersections between grain boundaries and test line. At least 200 grains and sub-grains with relatively clear boundaries are counted and calculated employing linear intercept method to estimate the average grain size. For those chips with elongated structures, the mean width (along small dimension) of grain is considered as the grain size [29].

Table 4 Test conditions

Parameters	Reference value
Spindle speed n (r/min)	25
Feed speed V_f (mm/r)	0.28
Cutting depth a_p (mm)	1.6
Ultrasonic amplitude A_y (μm)	0, 1, 2, 3
Ultrasonic frequency (kHz)	0, 21.71, 21.83, 22.15
Machining oil	SAE-30

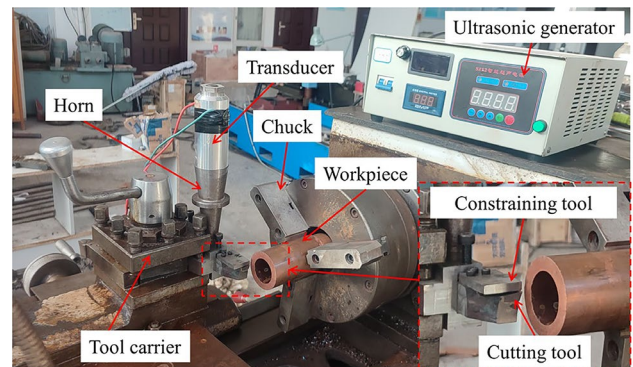


Fig. 8 Real experimental setup of the UCC

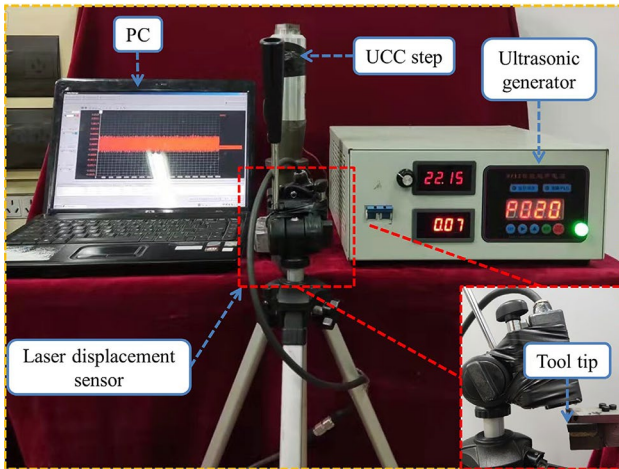
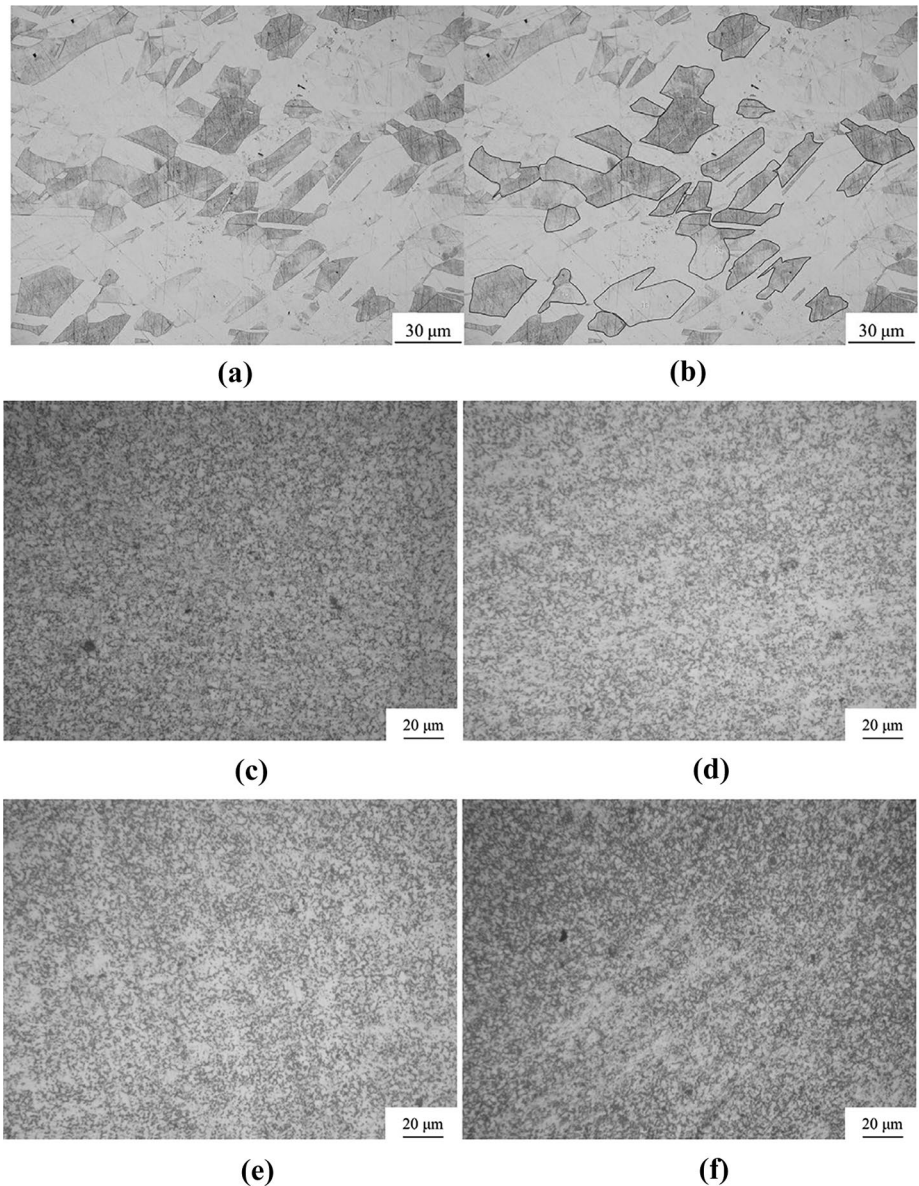


Fig. 9 Measurement of ultrasonic amplitude

The grain size distributions are shown in Fig. 11. The average values of the sample grains are 3.86 μm , 3.30 μm , 3.11 μm , and 2.66 μm , corresponding to the four amplitudes from 0 to 3 μm . The results show that the grain refinement of chip structure will gradually increase with the increase of ultrasonic amplitude. As the ultrasonic amplitude increases, the cutting strain rate will increase. The cutting strain rate directly affects the grain refinement of materials, and the strain rate is related to the mean free path of dislocation in materials. The larger the strain rate, the shorter the mean free path of dislocation, the smaller the size of dislocation cell, and the higher the degree of grain refinement. At the same time, the grain refinement process includes formation of dislocation walls through propagation, slip, annihilation, and recombination of the dislocations, and the wide grain will be divided into new fine grain.

Fig. 10 OM images of the **a** starting material, **b** IPP sample, **c** UCC sample for $A_Y = 0\mu\text{m}$, **d** UCC sample for $A_Y = 1\mu\text{m}$, **e** UCC sample for $A_Y = 2\mu\text{m}$, and **f** UCC sample for $A_Y = 3\mu\text{m}$



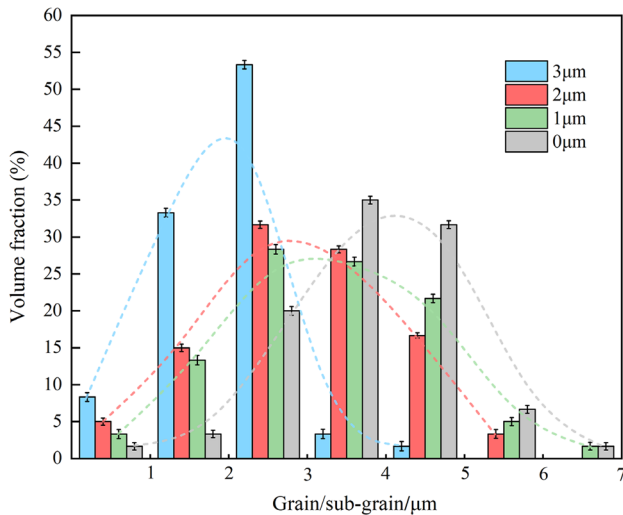


Fig. 11 Grain/sub-grain size statistic distributions of the UCC samples

In order to obtain more detail information about microstructure features, SEM technology is introduced. The SEM images of UCC samples are shown in Fig. 12. When the amplitude is 0 μm, the average grain size of the starting material is refined from 18.15 to 3.86 μm, indicating that TCC is an effective method to produce UFG pure copper. When the ultrasonic amplitude is 3 μm, the average grain size of the sample is about 69% of the TCC chip, indicating that ultrasonic vibration can significantly improve the efficiency of TCC. The results show that the strain rate in the deformation field can be increased by increasing the ultrasonic amplitude, and the grain size of chip will decrease.

4.3 Experimental results and analysis of microhardness

The microhardness of UCC samples with different ultrasonic amplitudes is shown in Fig. 13. The hardness of the starting material is 86 HV. The surface of UCC chip will produce work hardening, and the surface hardening will become larger with the increase of ultrasonic amplitude. The hardness of the UCC sample is 124 HV when the amplitude is 3 μm, which is about 8% higher than the hardness of TCC chip. The work hardening of the chip surface is closely related to the microstructure and dislocation density of the material [30]. The improvement concerning the strength or hardness of pure copper may be mainly attributed to the following: (i) grain refinement strengthening and (ii) dislocation strengthening.

Because the deformation resistance of grain boundary is very large, and the deformation of each grain will be restrained by the surrounding grains, so the hardness of pure copper chip always increases with the refinement of grain (i.e., the increase in the total area of grain boundaries). Therefore, the large enhancement in hardness of

UCC samples can be directly attributed to the grain refinement strengthening, one of the main strengthening mechanisms of material subjected to plastic deformation. Grain refinement strengthening is generally described by the Hall-Patch equation in which the strength of materials is inversely proportional to the grain size. Here, the hardness version is used instead of the flow stress version [31].

$$H_V = H_0 + K_H d^{-1/2} \tag{13}$$

where H_V is the hardness, H_0 and K_H are the material constants, and d is the average grain size of materials. Obviously, the hardness increases with the decreasing of the average grain size.

To examine the Hall-Patch relationship, the Vickers hardness values of the UCC samples in Fig. 13 are plotted as a function of $d^{-1/2}$, which is shown in Fig. 14. This indicates that the UCC samples follow the linear relationship described by Eq. (13). Accordingly, grain refinement strengthening makes significant contribution to the hardness enhancement of all the samples subjected to UCC.

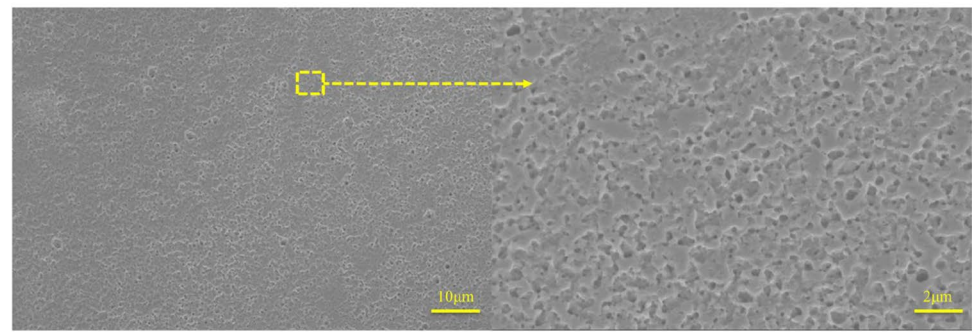
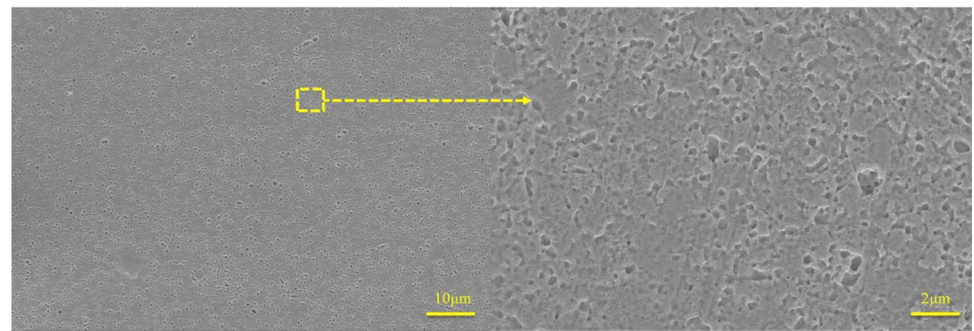
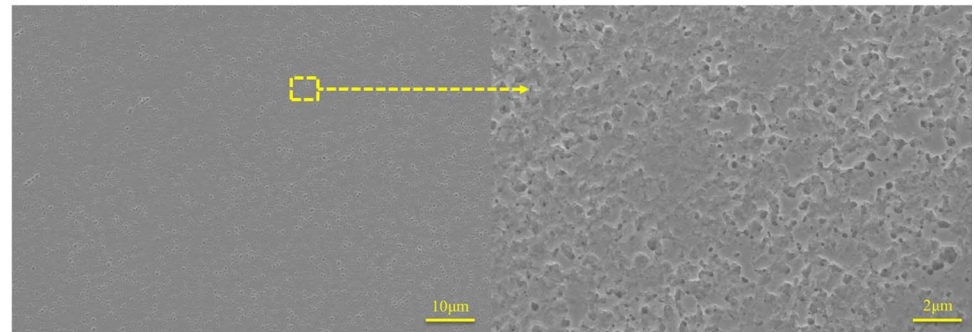
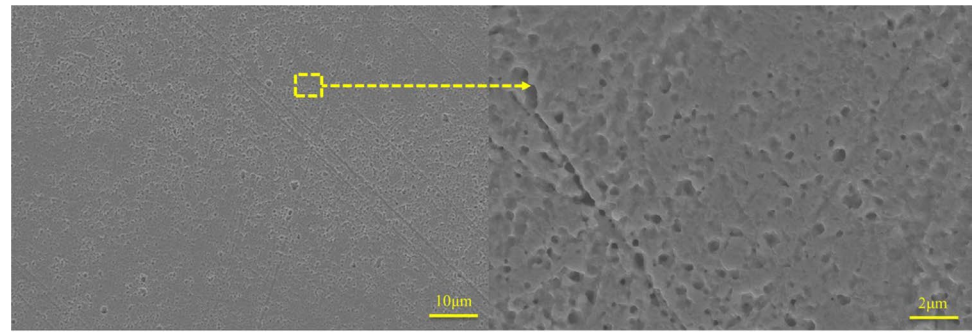
The dislocation strengthening, which is based on the prevention of dislocation slip and movement induced by interaction among dislocation, is another important strengthening mechanism that acts in materials. The high density of dislocation can decrease the mean free path of mobile dislocation, thus enhancing the resistance to deformation of materials. Because higher dislocation density in the UCC samples forms much more dislocation tangles, which act as barriers against the dislocation movement, thus hardening the materials. Theoretically, the contribution of dislocation to material strength can be described by the Bailey-Hirsch equation [32].

$$\sigma_d = M\alpha_D Gb\rho^{1/2} \tag{14}$$

where M is the Taylor factor, α_D is the strength coefficient, G is the shear modulus, b is the Burgers vector, and ρ is the dislocation density. Since the strength is proportional to the hardness of the materials, the higher the dislocation density, the greater the hardness of the materials.

The diffraction patterns of XRD for UCC samples are shown in Fig. 15a. In the XRD diffraction patterns, the dislocation density is mainly determined by the full width at half maximum (FWHM) of the diffraction peak [33, 34]. Figure 15b is the fitted peak of $A_Y = 3\mu\text{m}$; the corrected FWHM for peak is 0.2789° . When the amplitudes are 0 μm, 1 μm, and 2 μm, the corresponding FWHM are 0.23749° , 0.23948° , and 0.26345° , respectively. The XRD results show that the FWHM of peak increases with the increase of amplitude A_Y , and reaches the maximum when the amplitude is 3 μm. Therefore, ultrasonic vibration can improve the dislocation density of pure copper chip.

Fig. 12 SEM images and local enlarged drawing of the **a** UCC sample for $A_y = 0\mu\text{m}$, **b** UCC sample for $A_y = 1\mu\text{m}$, **c** UCC sample for $A_y = 2\mu\text{m}$, and **d** UCC sample for $A_y = 3\mu\text{m}$



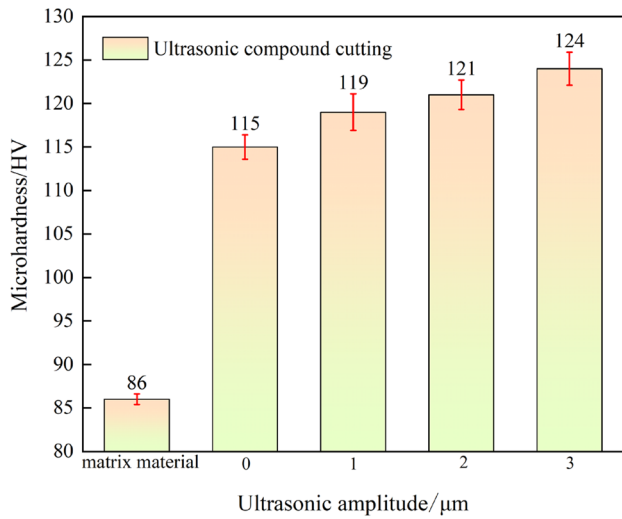


Fig. 13 Microhardness of UCC samples with different ultrasonic amplitudes

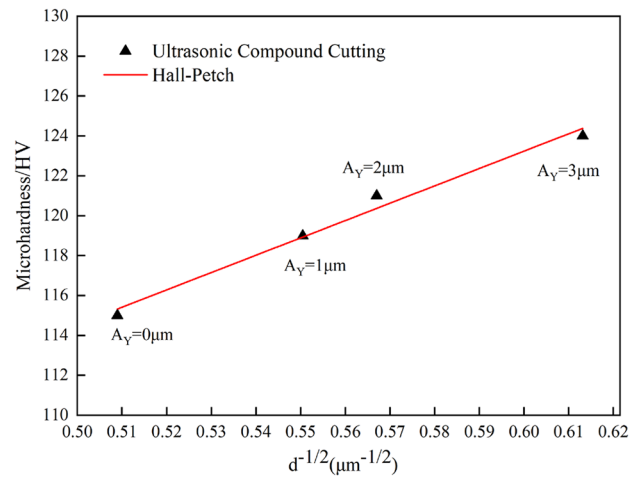


Fig. 14 Microhardness of samples processed by UCC as a function of $d^{-1/2}$

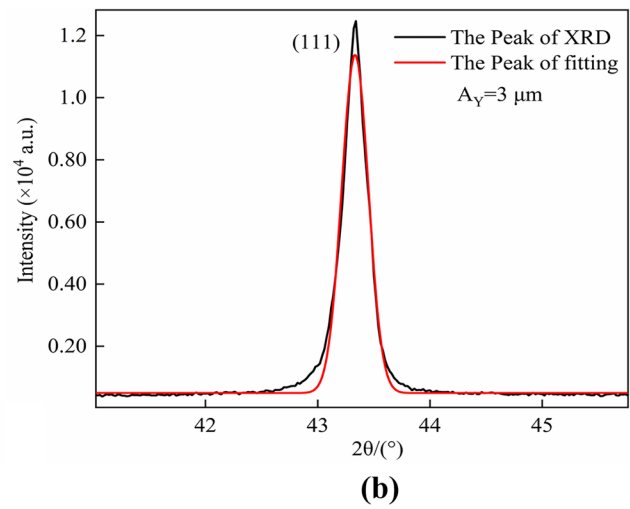
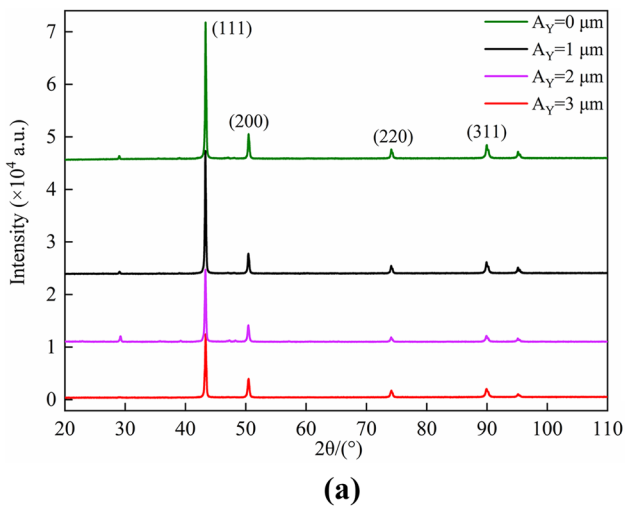


Fig. 15 XRD patterns: **a** UCC samples and **b** the fitted peak of $A_\gamma = 3\mu\text{m}$

5 Conclusions

In this paper, UCC was conducted with various amplitudes to investigate their comparative effects on chip microstructure and hardness of pure copper. The main observations could be summarized in following conclusions:

1. The cutting edge trajectory and strain rate model of UCC were discussed. The continuous cutting of TCC was transformed into intermittent cutting by UCC. Ultrasonic vibration along the cutting direction in UCC could increase the maximum strain rate $\dot{\epsilon}_{\max}$ in the primary shear zone.
2. A 3D finite element model of UCC was established. It could be obtained from the simulation results that the strain rate in the shear zone of UCC was significantly larger than that of TCC ($A_Y=0 \mu\text{m}$), and the maximum strain rate would gradually become larger with the increase of the amplitude A_Y .
3. The experimental results showed that the microstructure of the pure copper chip surface would change significantly if ultrasonic vibration was added to the TCC. The grain refinement and dislocation density of pure copper samples would increase with the increase of ultrasonic amplitude. In addition, the microhardness test showed that the hardening degree of chip surface would also be improved due to the grain refinement strengthening and dislocation strengthening.

Author contribution Haimeng Sun: conceptualization, methodology, writing—original draft. Feng Jiao: conceptualization, methodology, software, supervision. Ying Niu: resources, supervision, writing—review and editing. Zhuangfei Wang: software, investigation.

Funding This work was supported by the Natural Science Foundation of Henan (No. 202300410172) and Science and Technology Department of Henan Province (No. 212102210056) and National Natural Science Foundation of China (No. 51675164).

Declarations

Ethical approval This paper is new. Neither the entire paper nor any part of its content has been published or has been accepted elsewhere. It is not being submitted to any other journal as well.

Consent to participate Not applicable.

Consent for publication Not applicable.

Conflict of interest The authors declare no competing interests.

References

1. Qin L, Xie X, Li J (2017) Development status and future development trend of MEMS technology. *Mod Def Technol* 45(4):1–5. <https://doi.org/10.3969/j.issn.1009-086x.2017.04.001>
2. Yan G (2017) Deformation behavior and microstructure evolution of T-SHAPER micro-upsetting in ultrafine grained pure copper. Dissertation Harbin Inst Technol
3. Zhang J, Deng W, Liu L, Yin X, Xia W (2019) Study on forming extrusion cutting (FEC) producing fins and its forming performance. *J Mech Eng* 55(5):212–222. <https://doi.org/10.3901/JME.2019.05.212>
4. Ahmad K, Majid N, Omid I, Davood G, Kazem B, Fattah-alhosseini A (2021) Microstructural characterization and electrochemical behavior of nano/ultrafine grained pure copper through constrained groove pressing (CGP). *J Market Res* 11:1918–1931. <https://doi.org/10.1016/J.JMRT.2021.02.039>
5. Gholami M, Mhaede M, Pastorek F, Altenberger I, Hadzima B, Wollmann M, Wagner L (2016) Corrosion behavior and mechanical properties of ultrafine grained pure copper with potential as a biomaterial. *Adv Eng Mater* 18(4):615–623. <https://doi.org/10.1002/ADEM.201500269>
6. Akbarzadeh B, Gorji H, Jooybari MB, Jamaati R, Mirnia MJ (2021) Investigation of mechanical and microstructural properties of pure copper processed by combined extrusion-equal channel angular pressing (C-Ex-ECAP). *Int J Adv Manuf Technol* 113(7):2175–2191. <https://doi.org/10.1007/S00170-021-06692-5>
7. Luo J, Yu W, Xi C, Zhang C, Ma C (2019) Preparation of ultrafine-grained GH4169 superalloy by high pressure torsion and analysis of grain refinement mechanism. *J Alloy Compd* 777:157–161. <https://doi.org/10.1016/J.JALLCOM.2018.10.385>
8. Rahmatabadi D, Shahmirzaloo A, Hashemi R, Farahani M (2019) Using digital image correlation for characterizing the elastic and plastic parameters of ultrafine-grained Al 1050 strips fabricated via accumulative roll bonding process. *Mater Res Express* 6(8):086542. <https://doi.org/10.1088/2053-1591/AB18C3>
9. Ensafi M, Faraji G, Abdolvand H (2017) Cyclic extrusion compression angular pressing (CECAP) as a novel severe plastic deformation method for producing bulk ultrafine grained metals. *Mater Lett* 197(15):12–16. <https://doi.org/10.1016/J.MATLET.2017.03.142>
10. Brown TL, Saldana C, Murthy TG, Mann JB, Guo Y, Allard LF, King AH, Compton WD, Trumble KP, Chandrasekar S (2009) A study of the interactive effects of strain, strain rate and temperature in severe plastic deformation of copper. *Acta Mater* 57(18):5491–5500. <https://doi.org/10.1016/J.ACTAMAT.2009.07.052>
11. Moscoso W, Shankar MR, Mann JB, Compton WD, Chandrasekar S (2007) Bulk nanostructured materials by large strain extrusion machining. *J Mater Res* 22(1):201–205. <https://doi.org/10.1557/JMR.2007.0021>
12. Saldana C, Yang P, Mann JB, Moscoso W, Gill DD, Chandrasekar S, Trumble KP (2008) Micro-scale components from high-strength nanostructured alloys. *Mater Sci Eng* 503(1):172–175. <https://doi.org/10.1016/j.msea.2008.02.056>
13. Lou Y, He JS, Chen H, Long M (2017) Effects of vibration amplitude and relative grain size on the rheological behavior of copper during ultrasonic-assisted microextrusion. *Int J Adv Manuf Technol* 89(5):2421–2433. <https://doi.org/10.1007/S00170-016-9288-7>
14. Yang Z, Zhu L, Zhang G, Ni C, Lin B (2020) Review of ultrasonic vibration-assisted machining in advanced materials. *Int J Mach Tools Manuf* 156:103594. <https://doi.org/10.1016/j.ijmactools.2020.103594>
15. Ahmadi F, Farzin M, Meratian M, Loeian SM, Forouzan MR (2015) Improvement of ECAP process by imposing ultrasonic vibrations. *Int J Adv Manuf Technol* 79(1):503–512. <https://doi.org/10.1007/S00170-015-6848-1>
16. Zhang X, Zeng Y, Wang D, Wang T (2008) Surface hardening effectiveness on aluminium alloy 7075–T651 by ultrasonic shot peening. *Aeronaut Manuf Technol* 13:78–80. <https://doi.org/10.3969/j.issn.1671-833X.2008.13.014>

17. Cheng M, Xiao Y, Liu K, Zhang D (2019) Investigations on effects of ultrasonic rolling process on surface microstructure of steel. *Tool Eng* 53(7):73–76. <https://doi.org/10.3969/j.issn.1000-7008.2019.07.016>
18. Lu J, Wu X, Wu Z, Liu Z, Guo D, Lou Y, Ruan S (2017) microstructure and mechanical properties of ultrafine grained Al-6061 prepared using intermittent ultrasonic assisted equal-channel angular pressing. *J Mater Eng Perform* 26(10):1–11. <https://doi.org/10.1007/S11665-017-2946-6>
19. Bagherzadeh S, Abrinia K, Han Q (2020) Analysis of plastic deformation behavior of ultrafine grained aluminum processed by the newly developed ultrasonic vibration enhanced ECAP: simulation and experiments. *J Manuf Process* 50:485–497. <https://doi.org/10.1016/J.JMAPRO.2020.01.010>
20. Yin X, Deng W, Zou Y, Zhang J (2019) Ultrafine grained Al 7075 alloy fabricated by cryogenic temperature large strain extrusion machining combined with aging treatment. *Mater Sci Eng A* 762:138106. <https://doi.org/10.1016/J.MSEA.2019.138106>
21. Liu P (2017) Finite element simulation of ultrasonic vibration turning and parameter optimization. *Tool Eng* 51(1):31–36
22. Efe M, Moscoso W, Trumble KP, Compton WD, Chandrasekar S (2012) Mechanics of large strain extrusion machining and application to deformation processing of magnesium alloys. *Acta Mater* 60(5):2031–2042. <https://doi.org/10.1016/J.ACTAMAT.2012.01.018>
23. Guo Y, Efe M, Moscoso W, Sagapuram D, Trumble KP, Chandrasekar S (2011) Deformation field in large-strain extrusion machining and implications for deformation processing. *Scripta Mater* 66(5):235–238. <https://doi.org/10.1016/J.SCRIPTAMAT.2011.10.045>
24. Yin X (2020) Research on fabrication of ultrafine grained Al 7075 alloy via cryogenic temperature extrusion machining. Dissertation South China Univ Technol
25. Lin Q, Xie P, Hu J, Zhang F, Wang P, Wang Y (2021) Numerical simulation on dynamic damage evolution of high pure copper with different grain sizes. *Acta Physica Sinica* 70(20):113–121. <https://doi.org/10.7498/aps.70.20210726>
26. Dirras G, Ouarem A, Couque H, Gubicza J, Szommer P, Brinza O (2011) Microstructure and nanohardness distribution in a polycrystalline Zn deformed by high strain rate impact. *Mater Charact* 62(5):480–487. <https://doi.org/10.1016/J.MATCHAR.2011.03.002>
27. Kang JH, Torizuka S (2007) Dynamic recrystallization by large strain deformation with a high strain rate in an ultralow carbon steel. *Scripta Mater* 57(11):1048–1051. <https://doi.org/10.1016/J.SCRIPTAMAT.2007.07.039>
28. Liu S (2020) Evaluation and analysis on uncertainty of measuring metal average grain size by intersection point method. *Fail Anal Prev* 15(1):6–11. <https://doi.org/10.3969/j.issn.1673-6214.2020.01.002>
29. Swaminathan S, Shankar MR, Rao BC, Compton WD, Chandrasekar S, King AH, Trumble KP (2007) Severe plastic deformation (SPD) and nanostructured materials by machining. *J Mater Sci* 42(5):1529–1541. <https://doi.org/10.1007/S10853-006-0745-9>
30. Deng W, Li Q, Li B, Xie Z, He Y, Tang Y, Xia W (2014) Thermal stability of ultrafine grained aluminium alloy prepared by large strain extrusion machining. *Mater Sci Technol* 30(7):850–859. <https://doi.org/10.1179/1743284713Y.00000000421>
31. Su Q, Xu J, Li Y, Yoon JI, Shan D, Guo B, Kim HS (2018) Microstructural evolution and mechanical properties in superlight Mg-Li alloy processed by high pressure torsion. *Materials* 11(4):598. <https://doi.org/10.3390/MA11040598>
32. Ye C, Suslov S, Lin D, Liao Y, Cheng GJ (2014) Cryogenic ultrahigh strain rate deformation induced hybrid nanotwinned microstructure for high strength and high ductility. *J Appl Phys* 115(21):213519. <https://doi.org/10.1063/1.4881555>
33. Bai Q, Feng H, Si L, Pan R, Wang Y (2019) A novel stress relaxation modeling for predicting the change of residual stress during annealing heat treatment. *Metall Mater Trans A* 50(12):5750–5759. <https://doi.org/10.1007/S11661-019-05454-Z>
34. Takebayashi S, Kunieda T, Yoshinaga N, Ushioda K, Ogata S (2010) Comparison of the dislocation density in martensitic steels evaluated by some X-ray diffraction methods. *ISIJ Int* 50(6):875–882. <https://doi.org/10.2355/ISIJINTERNATIONAL.50.875>

Publisher's note Springer Nature remains neutral with regard to jurisdictional claims in published maps and institutional affiliations.